Phase-coherence dynamics of frequency-comb emission via high-order harmonic generation in few-cycle pulse trains

Chang-Tong Liang(梁畅通)[1,2,3], Jing-Jing Zhang(张晶晶)[1,2], and Peng-Cheng Li(李鹏程)[1,2,†]

[1] *Research Center for Advanced Optics and Photoelectronics, Department of Physics, College of Science, Shantou University, Shantou* 515063, *China*
[2] *Key Laboratory of Intelligent Manufacturing Technology of the Ministry of Education, Shantou University, Shantou* 515063, *China*
[3] *Institute of Applied Physics and Computational Mathematics, Beijing* 100088, *China*

(Received 30 September 2022; revised manuscript received 24 November 2022; accepted manuscript online 16 December 2022)

Frequency-comb emission via high-order harmonic generation (HHG) provides an alternative method for the coherent vacuum ultraviolet (VUV) and extreme ultraviolet (XUV) radiation at ultrahigh repetition rates. In particular, the temporal and spectral features of the HHG were shown to carry profound insight into frequency-comb emission dynamics. Here we present an *ab initio* investigation of the temporal and spectral coherence of the frequency comb emitted in HHG of He atom driven by few-cycle pulse trains. We find that the emission of frequency combs features a destructive and constructive coherences caused by the phase interference of HHG, leading to suppression and enhancement of frequency-comb emission. The results reveal intriguing and substantially different nonlinear optical response behaviors for frequency-comb emission via HHG. The dynamical origin of frequency-comb emission is clarified by analyzing the phase coherence in HHG processes in detail. Our results provide fresh insight into the experimental realization of selective enhancement of frequency comb in the VUV–XUV regimes.

Keywords: high-order harmonic generation, frequency comb, time-dependent Schrödinger equation, intense laser field systems

PACS: 32.80.Rm, 42.65.Ky, 42.50.Hz, 42.65.Re **DOI:** 10.1088/1674-1056/acac0f

1. Introduction

The rapid development of optical frequency comb based on femtosecond laser technique has had a huge impact on ultra-precision multidimensional spectroscopy, biology and medicine, and environmental sensing[1–3] in recent years. The spectrum of a frequency comb consists of a series of equally spaced teeth, *i.e.*, modes of a train of femtosecond pulses spaced by the repetition frequency of a mode-locked laser pulse.[4,5] By counting the number of teeth between an unknown optical frequency and an optical reference line, this comb is used as a fine ruler to measure an optical frequency instead of the corresponding wavelength, which can be determined much less precisely. Several approaches of synthesizing of optical frequency comb proposed have been provided the direct link between optic and microwave frequencies.[6–8] Some large-scale systems, such as free-electron laser-based x-ray generation and small-scale spectroscopy laboratories, can now measure or synthesize any optical frequency comb with extreme precision.[9,10] The femtosecond frequency-comb techniques are also promoting new frontiers in ultrafast science, such as providing a powerful new tool for observing the bound-state quantum electrodynamics, nanolithography technology, and x-ray atomic clocks with ultra-precision.[11–14] Extending these methods from vacuum ultraviolet (VUV) to extreme ultraviolet (XUV) spectral regions is highly desirable. For example, the optical frequency comb provides a new coherent XUV light source to allow novel precision quantum electrodynamics tests.[15–18]

Recently, there is a considerable interest in the generation of frequency comb both theoretically and experimentally.[19–21] Carrera *et al.*[22] have presented theoretically the behavior of the frequency-comb structure and coherence in VUV–XUV regimes via HHG in the laser pulse trains and investigated the role of electron correlation played in the structure and coherence of frequency comb HHG. Zhao *et al.* and Son *et al.*[23,24] have recently studied a theoretical extension of the many-mode Floquet theory for the nonperturbative treatment of the frequency-comb generation and suggest that the enhancement is due to the phenomenon of multiphoton resonance excitation of the excited states. Cingöz *et al.*[25] have explored the ultrahigh-precision spectroscopy of the 23rd harmonic of Xe and Kr atoms by using direct frequency comb spectroscopy in the XUV.[26] By utilizing intracavity HHG in a mode-locked oscillator with a Yb:YAG thin-disk laser medium, Kanda *et al.*[27] have demonstrated a novel method for realizing a MHz-repetition-rate coherent XUV light source. A novel experiment is single ion fluorescence excited with a single model of a UV frequency comb. Ozawa *et al.*[28] utilized this technology to improve the measurement uncertainty before using a continuous laser field. This suggests that the experimental observation of the frequency-comb structure in the VUV–XUV regimes will be-

†Corresponding author. E-mail: pchli@stu.edu.cn
© 2023 Chinese Physical Society and IOP Publishing Ltd

come feasible when the spectral resolution is improved. Thus theoretical exploration of the generation of frequency comb via HHG, including the spectral enhancement and coherence dynamics related to the quantum trajectories, is a timely and important subject to study, providing new advancement for the coherent VUV–XUV radiation with ultrahigh repetition rates.[29,30]

In this work, we advance this field by presenting an *ab initio* study of the dynamical origin of suppression and enhancement of frequency-comb emission in HHG obtained from helium atom in intense mid-infrared laser pulse trains by solving the three-dimensional time-dependent Schrödinger equation (TDSE) accurately and efficiently by means of the time-dependent generalized pseudospectral (TDGPS) method.[31] In calculation, we adopt a helium atom. The He atom has been chosen particularly as the atomic medium for the generation of frequency comb via HHG, since the He atom possesses a deep ionization potential, which allows one to tolerate intense laser pulse trains, leading to the stable harmonic emission. For a proper account of the high ionization energy of He, an accurate angular momentum-dependent model potential is constructed for accurate atomic-structure calculation.[31] We find that spectral coherence on frequency-comb emission via HHG plays an important role. We uncover the dynamical regime of the nested comb structure with clearly distinguishable harmonic peaks of different intensities, they have the unique phase-coherent modes generated by different laser pulses. Furthermore, by comparing the exclusively phase-locked regular harmonics, we reveal intriguing and substantially different nonlinear optical response behaviors. Moreover, we clarify the dynamical origin of suppression and enhancement of frequency-comb by using the analysis of quantum trajectories. Our study provides a deeper understanding of the mechanisms for the suppression and enhancement of frequency-comb emission in HHG.

2. Theoretical methods

The harmonic spectrum of the atom can be calculated accurately and efficiently by solving the TDSE. The TDSE can be written in the dipole approximation in atomic unit (a.u.) as

$$\mathrm{i}\frac{\partial\psi(\boldsymbol{r},t)}{\partial t}=[H_0+V(\boldsymbol{r},t)]\psi(\boldsymbol{r},t), \tag{1}$$

where $V(\boldsymbol{r},t)$ is the time-dependent atom–field interaction, which has the following form:

$$V(\boldsymbol{r},t)=-E(t)\boldsymbol{F}\cdot\boldsymbol{r}=-E(t)Fz. \tag{2}$$

The H_0 represents the unperturbed atom Hamiltonian, it can be written as

$$H_0=-\frac{1}{2}\nabla^2+\sum_l|\mathrm{Y}_l^0\rangle V_l\langle\mathrm{Y}_l^0|, \tag{3}$$

where V_l is the model potential for He, and Y_l^0 is a spherical harmonic. In order to obtain the accurate calculation of the harmonic spectra of He, an angular-momentum-dependent model potential is constructed as the following form:

$$V_l=-\frac{\alpha}{2r^4}W_6\left(\frac{r}{r_\mathrm{c}}\right)-\frac{1}{r}-\left(\frac{N-S}{r}+A\right)\mathrm{e}^{-B_1r}-\frac{S}{r}\mathrm{e}^{-B_2r}, \tag{4}$$

where α is the He^+ core dipole polarizability, W_6 is a core cutoff function given by

$$W_n(x)=1-\left[1+nx+\frac{(nx)^2}{2!}+\cdots+\frac{(nx)^2}{n!}\right]\mathrm{e}^{-nx}, \tag{5}$$

and r_c is an effective He^+ core radius. In the present work we find it is sufficient to use five different angular-momentum-dependent model potential, namely, all for states with $l=0,1,2,3$ and $l\geq 3$. The parameters of V_l used are the same as Ref. [32].

In the frequency domain, the femtosecond pulse train emitted by a laser oscillator of length L has a repetition frequency f_r, which is inversely proportional to the round trip time T of the laser in the oscillating cavity, $T=L/f_\mathrm{r}$. Since the group and phase velocities inside the cavity are not equal, there is a phase shift $\Delta\phi$ from pulse to pulse. Assuming that the pulse envelope produced by the laser has an ideal repetition period and the phase difference between the carrier and the envelope remains constant in each period, the frequency comb ω_m can be expressed as: $\omega_n=n\omega_\mathrm{r}+\omega_\delta$, where n is an integer index and typically on the order of 10^5–10^6. The electric field for a train of pulses in the time domain is expressed by

$$E(t)=\sum_{n=1}^{N}E(t-n\tau)\exp[\mathrm{i}(\omega_\mathrm{c}t-n\omega_\mathrm{c}\tau+n\Delta\phi)], \tag{6}$$

where ω_c is the carrier frequency, τ is the pulse separation, and N is the number of pulses. The pulse-to-pulse phase shift is given by $\Delta\phi$.

The TDSE is solved by means of the TDGPS method.[31,33] It has been shown that the TDGPS is considerably more accurate and computationally more efficient than the conventional time-dependent propagation techniques using equal-spacing grid discretization. The TDGPS method has been applied successfully to the study of a broad range of multiphoton ionization and HHG of atomic and molecular systems in strong fields. The numerical scheme of the TDGPS method consists of two essential steps: (i) The spatial coordinates are optimally discretized in a nonuniform spatial grid by the generalized pseudospectral technique.[33] This discretization uses only a modest number of grid points, and it is characterized by denser grids near the nuclear origin and sparser grids for larger distances. (ii) A second-order split-operator technique in the energy representation is used for the time propagation of the wave function, which can be expressed as

$$\psi(\boldsymbol{r},t+\Delta t)\simeq\exp\left(-\mathrm{i}H_0\frac{\Delta t}{2}\right)$$

$$\times \exp\left[-\mathrm{i}V(\boldsymbol{r},t+\frac{\Delta t}{2})\Delta t\right]$$
$$\times \exp\left(-\mathrm{i}H_0\frac{\Delta t}{2}\right)\psi(\boldsymbol{r},t)+O(\Delta t^3). \quad (7)$$

When the time-dependent wave function $\psi(\boldsymbol{r},t)$ is available, we can calculate the expectation value of the induced dipole moment in the length and acceleration forms, which can be written as

$$d_{\mathrm{L}}(t) = \langle\psi(\boldsymbol{r},t)|z|\psi(\boldsymbol{r},t)\rangle, \quad (8)$$
$$d_{\mathrm{A}}(t) = \frac{\partial^2}{\partial t^2}\langle\psi(\boldsymbol{r},t)|z|\psi(\boldsymbol{r},t)\rangle = \langle\psi(\boldsymbol{r},t)|[H,[H,z]]|\psi(\boldsymbol{r},t)\rangle, \quad (9)$$

respectively. The HHG spectrum can be calculated, within the semiclassical approach, by the following expression:[34]

$$S(\omega)=\frac{2\omega^4}{3\pi c^3}|\widetilde{d}(\omega)|^2=\frac{2}{3\pi c^3}|\widetilde{a}(\omega)|^2, \quad (10)$$

where c is the speed of light, $\widetilde{d}(\omega)$ and $\widetilde{a}(\omega)$ are the Fourier transforms of the time-dependent dipole moment in the length and acceleration forms, given by

$$\widetilde{d}(\omega)=\int_{-\infty}^{\infty} d_L(t)\,\mathrm{e}^{-\mathrm{i}\omega t}\,\mathrm{d}t, \quad (11)$$
$$\widetilde{a}(\omega)=\int_{-\infty}^{\infty} d_A(t)\,\mathrm{e}^{-\mathrm{i}\omega t}\,\mathrm{d}t, \quad (12)$$

respectively.

To investigate the structural characteristics of HHG produced by helium atom driven by high frequency laser fields, the harmonic spectral density is analyzed by phase spectrum, and the specific expression is as follows:

$$S(\omega)=\frac{1}{N}\sum_{n=1}^{N}S_n(\omega). \quad (13)$$

Here $S_n(\omega)$ is the HHG spectrum by one-pulse case,[35]

$$S_n(\omega) = \frac{1}{\tau\omega^2}\int_{(n-1)\tau}^{n\tau} d_L(t)\,\mathrm{e}^{-\mathrm{i}\omega t}\,\mathrm{d}t = |S_n(\omega)|\,\mathrm{e}^{-\mathrm{i}S_t(\omega)}, \quad (14)$$

where τ is the time interval between five laser pulses, and $S_t(\omega)$ denotes spectral phase.

3. Results and discussion

3.1. Enhancement and suppression of frequency comb generation in HHG

In Fig. 1(a), we present the driving laser field composed of five successive pulses. The laser parameter used is the 1800-nm mid-infrared laser wavelength, with 30-fs full width at half maximum (FWHM) Gaussian laser pulses, and the peak intensity is $I = 1.8\times10^{13}$ W/cm^2. Figure 1(b) shows an enlarged view of the laser field $E(t)$ for one pulse. Figure 1(c) shows the HHG spectrum of the He atom driven by five laser pulses separated by $\tau = 0.3$ ps. The time delay between pulses allows to expedite the numerical calculation and will not affect the coherence of the harmonics. Figures 1(d), 1(e), and 1(f) indicate the detailed view of the nested comb structure in the vicinity of near-threshold, plateau, and near-cutoff harmonics, respectively. These enlarged views of the harmonics show the different features in the vicinity of the 43rd order harmonic (H43), the 59th order harmonic (H59), and the 82nd order harmonic (H82).

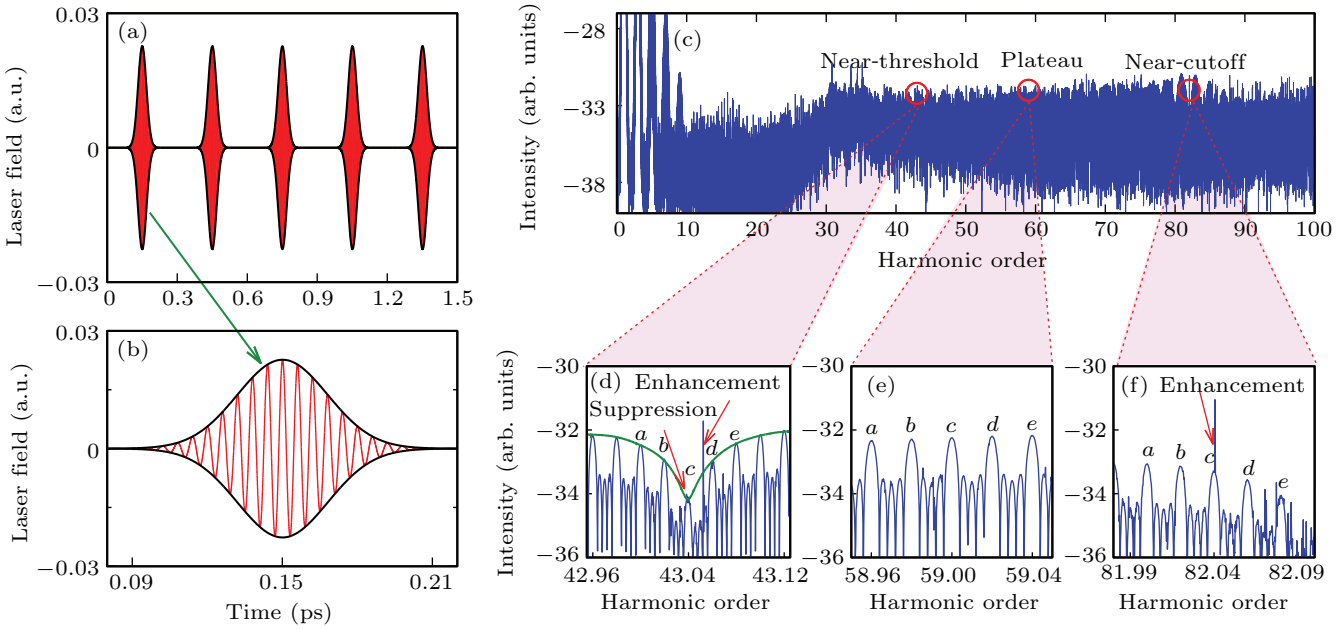


Fig. 1. (a) Laser field composed of five successive 30-fs FWHM Gaussian laser pulses. (b) An enlarged view of one pulse. (c) HHG spectrum $S(\omega)$ generated by the five successive pulses. Panels (d), (e), and (f) show the detailed view of the nested comb structure in the vicinity of near-threshold, plateau, and near-cutoff harmonics, respectively.

It is clearly seen that the HHG spectra from the near-threshold harmonic to the cutoff has a nested comb structure in the frequency domain space, namely, the overall structure of the harmonic is composed of many interval nested peaks, among which a group of peaks contains two higher peaks, two sub-peaks, and a lower peak. That means a nested comb structure is formed within each harmonic order. However, this nested comb structure shows a minima near H43 indicated by the red arrow. This means that there is a suppression of frequency-comb emission in HHG. For the comparison, these comb peaks in the different regions are marked by *a*, *b*, *c*, *d*, and *e* as shown in Figs. 1(d)–1(f), respectively. In addition, in Figs. 1(d) and 1(f), we find two sharp enhancements of frequency-comb emission at near-threshold and near-cutoff regions. Two sharp enhancement of frequency-comb emission are located near H43 and H82 indicated by the red arrows, respectively. The abnormal enhancements from near threshold to cutoff are produced due to the huge phase changing in HHG for the laser pulse trains. The quantum dynamics will be discussed in the next section.

3.2. Phase-coherence dynamics of frequency-comb emission

To understand the suppression (Suppr.) or enhancement (Enhan.) of frequency-comb emission in HHG, we analyze the harmonic phase of the peaks marked by *a*, *b*, *c*, *d*, and *e* as shown in Figs. 1(d)–1(f). The results are shown in Fig. 2. We find that the harmonic phases of the peaks have been changed sharply at H43.04, H43.05, and H82.04 when the number of pulses is adding. For each sharp change of the harmonic phase of the peaks, there is just a corresponding suppression or enhancement of frequency-comb emission in HHG. This implies that the harmonic phase of each pulse plays an important role. In addition, we find that the sharp phase changes of the HHG are located at near-threshold and near-cutoff regions in HHG, while the harmonic phase in plateau changes a little, which evidently shows the regular frequency-comb structure comes from the phase locking. In other words, these equally spaced discrete frequencies are essentially caused by constructive quantum interference emanating from the phase-locked induced dipole moments. These suppressions and enhancements can be understood by the spectral phase interferences among induced dipole pulses, which depends on the pulse number N. Note that HHG processes occur over the duration of each individual pulse cycle only which is a much smaller time scale than the separation between successive pulses generated by a mode-locked femtosecond laser with a repetition frequency. Hence, the emitted HHG radiation should not be appreciably affected by the delay between pulses.[19] Next, we perform an analysis of the coherence properties of the HHG comb structure with the number of pulses for a better understanding of the origin of harmonic comb generation.

Figure 3(a) shows the evolution of the harmonic spectral phases with the number of pulses in the vicinity of the near-threshold. The blue line represents the phase for the first dipole pulse $N = 1$, green line for $N = 2$, and purple-red line for $N = 3$, which can be obtained by Eq. (14). The insets show a detailed view of harmonic spectral phases for the different numbers of the pulses. With increasing the number of laser pulses, the interference of HHG from the different pulse trains becomes more and more complex, leading to the third pulse start to make a big difference. The suppression and sharp enhancement will occur due to the sudden oscillation of the phases of the larger number ($N = 3$) of dipole pulses. Figure 3(b) shows the evolution of the harmonic spectral phases with the number of pulses in the vicinity of the plateau. We find that constructive interference will occur only if the phases of individual dipole pulses are identical and intersect at the color dots where the comb positions are located at the corresponding frequency comb spectra. These quantum-phase interferences are responsible for the comb structure in all the harmonics. In the vicinity of the cutoff, similar results have been shown in Fig. 3(c), the sudden oscillation of the phases of the number ($N = 2, 3$) of dipole pulses leads to the sharp enhancement of frequency-comb emission. Based on the interference of HHG from the different pulse trains, the enhanced harmonic order will be changed when the number of the laser pulse is added.[20]

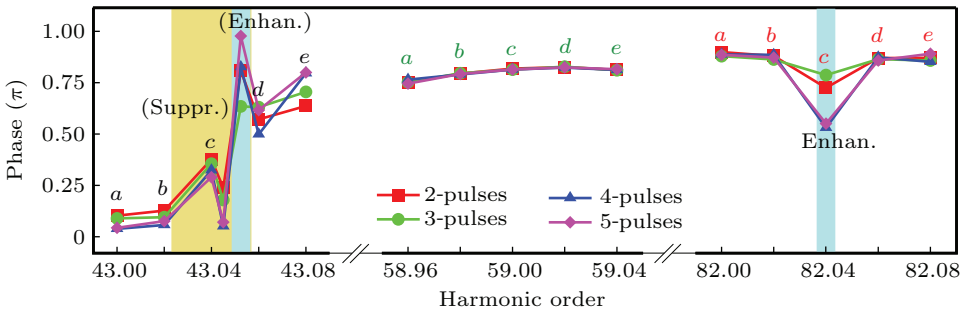


Fig. 2. Harmonic spectral phase of the peaks marked by *a*, *b*, *c*, *d*, and *e* as shown in Figs. 1(d)–1(f). The labels with different color indicate the results when the number of pulses is adding. The laser parameters used are the same as those in Fig. 1.

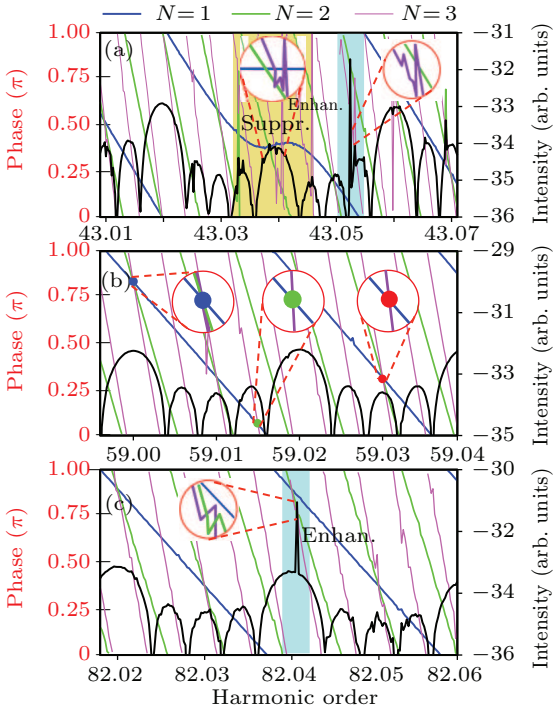


Fig. 3. Evolution of the harmonic spectral phases with the number of pulses in the vicinity of near-threshold, plateau, and near-cutoff regions, respectively. (a) H43.04. (b) H59.02. (c) H82.04. The blue line represents the phase for the first dipole pulse $N = 1$, green line for $N = 2$, and purple-red line for $N = 3$. All lines intersect at the color dots indicating the comb positions. The insets show a detailed view of the interference of harmonic spectral phases for the different numbers of the pulse. Other laser parameters used are the same as those in Fig. 1.

3.3. Spectral and temporal resolved dynamics of the frequency-comb generation

To understand the ionization feature in frequency-comb HHG emission, we calculated the ionization probability of the five pulses, given by

$$P_{\text{ion}}(t) = 1 - \langle \psi(\boldsymbol{r},t) | \psi(\boldsymbol{r},t) \rangle. \tag{15}$$

The result is shown in Fig. 4(a). In Fig. 4(a), a uniform staircase pattern visibly depicts the overall appearance of the ionization probability once the laser pulse train is completed. The ionization probability changes rapidly during each of the pulse peak intensities. Beyond the intensity of the pulse peak, the ionization probability reaches an ionization plateau region until the next pulse comes to interact with the atom. In relatively weak laser intensities, where minimal ionization takes place and the neutral atom lingers as the dominant species, the laser field sees nearly the same population on the ground state. Hence, the ionization probability after each consecutive pulse remains nearly equal. In general, in the single-atom level case, the ionization probability depends on the laser intensity.[36] For a higher laser intensity, the ionization probability will be increased and finally reaches saturation with adding the laser pulse numbers.[35]

Figure 4(b) shows the wavelet transform of time-frequency spectra of frequency-comb HHG driven by the five laser pulses. The white dashed lines indicate that the given orders for several harmonics of H43.04, H59, and H82.04 as shown in Fig. 1. The result shows that the time-frequency spectral of frequency-comb HHG is similar during each of the laser pulses. Figures 4(c), 4(d), and 4(e) show the time profiles of the H43.04, H59, and H82.04 harmonics obtained by the cross-section of the time-frequency spectral of frequency-comb HHG shown in Fig. 4(b) at a given harmonic frequency. The corresponding dynamical phase $\theta(t_{\text{q}})$ is therein extracted from the wavelet transform of the induced dipole $d_\omega(t_{\text{q}})$, given by[21]

$$d_\omega(t_{\text{q}}) = |d_\omega(t_{\text{q}})| \, \mathrm{e}^{-\mathrm{i}[(\omega t_{\text{q}} + \theta(t_{\text{q}})]}. \tag{16}$$

The results are denoted by red dots as shown in Figs. 4(c)–4(e), respectively. According to the three-step semiclassical model,[37] as the electron returning energy is located at before cutoff, there exists two returning trajectories: the first short trajectory returns at a dynamical phase less than 342° (or 162°), and the second long trajectory at a phase larger than 342° (or 162°).[38] This is also confirmed in Figs. 4(c) and 4(d). The time profile near the cutoff only excites one burst within each half-optical cycle (o.c.), where the short and long trajectories have the synchronous recollision of the electronic wave packet with the ionic core as shown in Fig. 4(e). Figure 4(c) shows the time profile of the H43.04 in the vicinity of the near-threshold ionization. The time profile exhibits a complex pattern within each optical cycle. Figure 4(d) shows the time profile of the H59 harmonics in the vicinity of the plateau. It has regular long and short trajectories for each laser pulse. This also can be confirmed by the dynamical phases obtained from the wavelet transform of the induced dipole, corresponding to each instant t_{q} of electron–ion core recollision. The dynamical phases $\theta(t_{\text{q}})$ of the cutoff harmonics in Fig. 4(e) show a time profile mimicking the laser pulse shape during each pulse train, which indicates that the long and short trajectories are synchronous in the frequency-comb HHG emission process during each laser pulse. In Fig. 4(d), we find that the long trajectory has stronger phase dependence on laser intensity than that of the short one. It is seen that the long and short trajectories have their emission step and that this step remains constant in successive laser pulse trains. However, in near-threshold regions, the dynamical phase becomes more complex, which means that the interference of the quantum trajectories increases as shown in Fig. 4(b). Combining the quantum trajectories and dynamical phase analysis, we find that the quantum trajectories interference is greatest in the near-threshold region, which leads to the frequency-comb structure easily occurring suppression and enhancement. The quantum trajectories interference in near-plateau and near-cutoff regions is the most stable. Thus different quantum trajectories have their emission steps that take place steady interference

in the five laser pulse trains leading to the regular frequency comb near the plateau region. Near the cutoff regions, when some phases of quantum trajectories have a sharp change due the large relaxation effects of the electron, leading a huge enhancement structure thanks to constructive interference of the contributing quantum trajectories. Therefore, we think that the enhanced interference can be modulated by using a constant phase relationship of frequency comb in HHG emission among successive laser pulse trains.

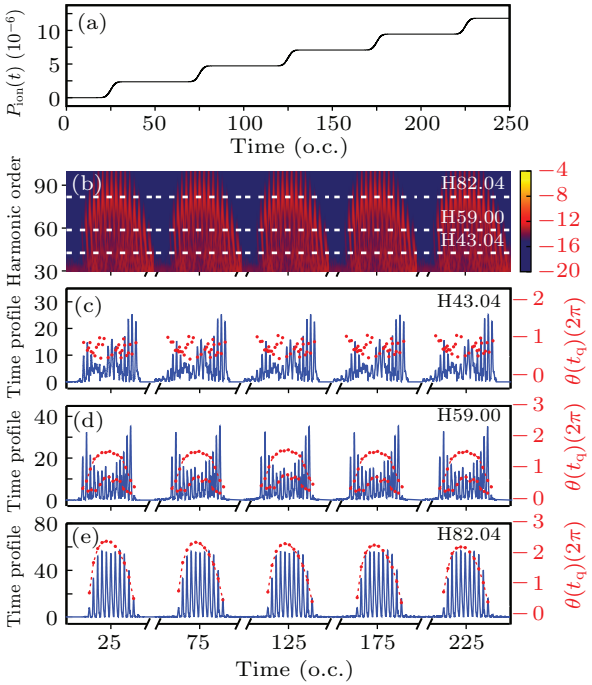


Fig. 4. (a) Ionization probability of the He atom obtained from five laser pulses. (b) The wavelet time–frequency spectrum of frequency-comb HHG. Panels (c), (d), and (e) are the time profiles of the specific harmonic of H43.04, H59.00, and H82.04, respectively. The red dots are the dynamical phases. The laser parameters used are the same as those in Fig. 1.

4. Conclusion

We have presented a detailed investigation of the mechanism of the suppression and enhancement of frequency-comb emission via HHG of the He atom. The HHG power spectrum is obtained by accurately solving the TDSE. The numerical procedure involves the novel TDGPS method for optimal spatial discretization of the Hamiltonian and efficient time propagation of the time-evolution operator. Our analysis reveals that the induced dipole moments of different pulses interfere in time with opposite phases, so their contributions are canceled out in the total dipole moment. Therefore, the destructive interference of frequency-comb emission has been observed in near-threshold HHG. This is an unexpected observation for the frequency-comb emission. In addition, the frequency-comb emission in HHG also shows a constructive interference in near-threshold HHG and cut-off harmonics. In fact, the underlying physical effect that causes this destructive or constructive phase interference in a specific comb line is the competition between the Coulomb field and the laser field. Because this competition leads to the phase difference of quantum trajectories related to the HHG. Combining with the quantum trajectories and the dynamical emission features analysis, we have provided a clear physical picture for the enhancement and suppression structure generation.

Although our result is for the single-atom level case, the insights obtained are quite general and still applicable for the understanding of phase-coherence dynamics of frequency-comb emission via HHG in few-cycle pulse trains, because the previous findings show that the commonly used the low pressure, small laser intensity and loose pulse waist. That is to say, the laser-field shape is not modified through the medium, because the density of free electrons determined by the total ionization probabilities is very small. So, the generation of frequency comb still is observable. However, according to our previous works,[36] in higher laser intensity, there is a difference between the macroscopic HHG spectra and the single-atom case because of the stronger ionization. Therefore, our results carry fresh insight and suggest that the experimental observation for a selective enhancement of the frequency comb via HHG will become feasible in the future.

Acknowledgements

Peng-Cheng Li would like to offer special gratitude to Prof. Shih-I Chu (University of Kansas) for helpful discussion.

Project supported by the National Natural Science Foundation of China (Grant Nos. 12074239 and 91850209), the Natural Science Foundation of Guangdong Province, China (Grant Nos. 2020A1515010927 and 2020ST084), the Fund from the Department of Education of Guangdong Province, China (Grant Nos. 2019KTSCX038 and 2020KCXTD012), and the Fund from Shantou University (Grant No. NTF18030).

References

[1] Picqué N and Hänsch T W 2019 *Nat. Photon.* **13** 146
[2] Foltynowicz A, Ban T, Masłowski P, Adler F and Ye J 2011 *Phys. Rev. Lett.* **107** 233002
[3] Bergevin J, Wu T H, Yeak J, Brumfield B E, Harilal S S, Phillips M C and Jones R J 2018 *Nat. Commun.* **9** 1273
[4] Jones D J, Diddams S A, Ranka J K, Stentz A, Windeler R S, Hall J L and Cundiff S T 2000 *Science* **288** 635
[5] Reichert J, Holzwarth R, Udem Th and Hänsch T W 1999 *Opt. Commun.* **172** 59
[6] Diddams S A, Vahala K and Udem Th 2020 *Science* **369** 6501
[7] Diddams S A, Jones D J, Ye J, Cundiff S T and Hall J L 2000 *Phys. Rev. Lett.* **84** 5102
[8] Dai S Y, Li K Q, Zhai Y Y, Xia W, Wang Q, Xiong W, Qi X H and Chen X Z 2017 *Chin. Phys. Lett.* **34** 013201
[9] Dreissen L S, Roth C, Gründeman E L, Krauth J J, Favier M and Eikema K S E 2019 *Phys. Rev. Lett.* **123** 143001
[10] Coddington I, Newbury N and Swann W 2016 *Optica* **3** 414

[11] Hernández-García C, Pérez-Hernández J A, Popmintchev T, Murnane M M, Kapteyn H C, Jaron-Becker A, Becker A and Plaja L 2013 *Phys. Rev. Lett.* **111** 033002

[12] Eckle P, Smolarski M, Schlup P, Biegert J, Staudte A, Schöffler M, Muller H G, Dörner R and Keller U 2008 *Nat. Phys.* **4** 565

[13] Oskay W H, Diddams S A, Donley E A, Fortier T M, Heavner T P, Hollberg L, Itano W M, Jefferts S R, Delaney M J, Kim K, Levi F, Parker T E and Bergquist J C 2006 *Phys. Rev. Lett.* **97** 020801

[14] Altmann R K, Galtier S, Dreissen L S and Eikema K S E 2016 *Phys. Rev. Lett.* **117** 173201

[15] Matveev A, Parthey C G, Predehl K, Alnis J, Beyer A, Holzwarth R, Udem Th, Wilken T, Kolachevsky N, Abgrall M, Rovera D, Salomon C, Laurent P, Grosche G, Terra O, Legero Th, Schnatz H, Weyers S, Altschul B and Hänsch T W 2013 *Phys. Rev. Lett.* **110** 230801

[16] Hölsch N, Beyer M, Salumbides E J, Eikema K S E, Ubachs W, Jungen C and Merkt F 2019 *Phys. Rev. Lett.* **122** 103002

[17] Krausz F and Ivanov M 2009 *Rev. Mod. Phys.* **81** 163

[18] Chini M, Zhao K and Chang Z H 2014 *Nat. Photon.* **8** 178

[19] Carrera J J, Son S K and Chu S I 2008 *Phys. Rev. A* **77** 031401R

[20] Tudorovskaya M and Lein M 2017 *Phys. Rev. A* **95** 043418

[21] Li P C, Sheu Y L, Laughlin C and Chu S I 2015 *Nat. Commun.* **6** 7178

[22] Carrera J J and Chu S I 2009 *Phys. Rev. A* **79**, 063410

[23] Zhao D, Li F L and Chu S I 2013 *Phys. Rev. A* **87** 043407

[24] Son S K and Chu S I 2008 *Phys. Rev. A* **77** 063406

[25] Cingöz A, Yost D C, Allison T K, Ruehl A, Fermann M E, Hartl I and Ye J 2008 *Nature* **482** 68

[26] Lee J, Carlson D R and Jones R J 2008 *Opt. Express* **19** 23315

[27] Kanda N, Imahoko T, Yoshida K, Tanabashi A, Eilanlou A A, Nabekawa Y, Sumiyoshi T, Kuwata-Gonokami M and Midorikawa K 2020 *Light Sci. Appl.* **9** 168

[28] Ozawa A, Davila-Rodriguez J, Bounds J R, Schuessler H A, Hänsch T W and Udem Th 2017 *Nat. Commun.* **8** 44

[29] Chini M, Wang X W, Cheng Y, Wang H, Wu Y, Cunningham E, Li P C, Heslar J, Telnov D A, Chu S I and Chang Z H 2014 *Nat. Photon.* **8** 437

[30] Rohwer T, Hellmann S, Wiesenmayer M, Sohrt C, Stange A, Slomski B, Carr A, Liu Y W, Avila L M, Kalläne M, Mathias S, Kipp L, Rossnagel K and Bauer M 2011 *Nature* **471** 490

[31] Tong X M and Chu S I 1997 *Chem. Phys.* **217** 119

[32] Li P C, Laughlin C and Chu S I 2014 *Phys. Rev. A* **89** 023431

[33] Li P C and Chu S I 2020 *Chin. Phys. B* **29** 083202

[34] Li P C, Sheu Y L, Laughlin C and Chu S I 2014 *Phys. Rev. A* **90** 041401R

[35] Liang C T, Wu Y Y, Wang Z B and Li P C 2022 *Opt. Express* **30** 2413

[36] Li P C and Chu S I 2013 *Phys. Rev. A* **88** 053415

[37] Corkum P B 1993 *Phys. Rev. Lett.* **71** 1994

[38] Tong X M and Chu S I 2000 *Phys. Rev. A* **61** 021802(R)